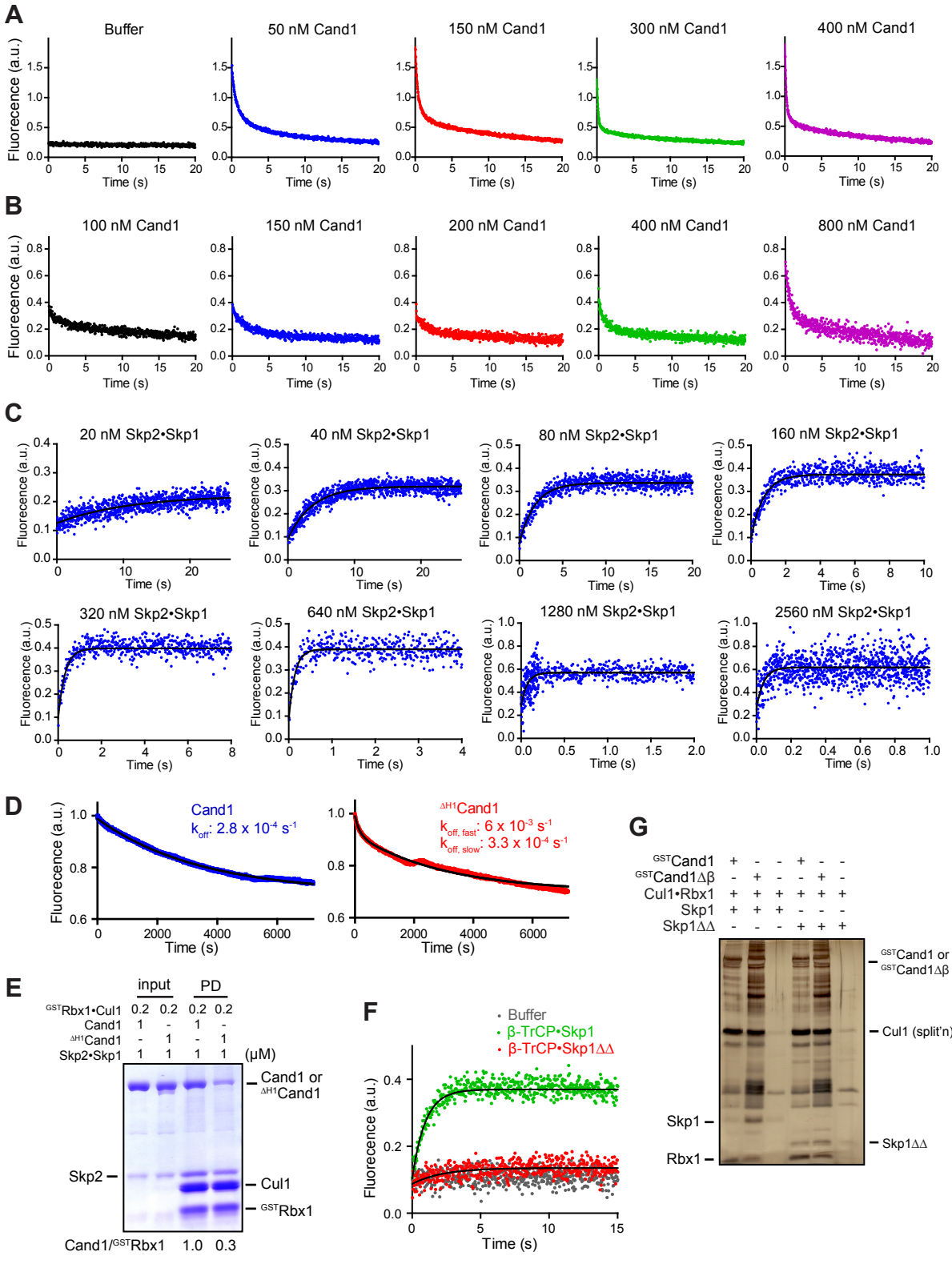
A
Buffer
50 nM Cand1
150 nM Cand1
300 nM Cand1
400 nM Cand1
Fluorescence (a.u.)
Time (s)
B
100 nM Cand1
150 nM Cand1
200 nM Cand1
400 nM Cand1
800 nM Cand1
C
20 nM Skp2•Skp1
40 nM Skp2•Skp1
80 nM Skp2•Skp1
160 nM Skp2•Skp1
320 nM Skp2•Skp1
640 nM Skp2•Skp1
1280 nM Skp2•Skp1
2560 nM Skp2•Skp1
D
Cand1
k_off: 2.8 x 10^-4 s^-1
ΔH1Cand1
k_off, fast: 6 x 10^-3 s^-1
k_off, slow: 3.3 x 10^-4 s^-1
E
input
PD
GSTRbx1•Cul1
Cand1
ΔH1Cand1
Skp2•Skp1
(μM)
Cand1 or ΔH1Cand1
Skp2
Cul1
GSTRbx1
Cand1/GSTRbx1 1.0 0.3
F
Buffer
β-TrCP•Skp1
β-TrCP•Skp1ΔΔ
G
GSTCand1
GSTCand1Δβ
Cul1•Rbx1
Skp1
Skp1ΔΔ
GSTCand1 or GSTCand1Δβ
Cul1 (split'n)
Skp1
Rbx1
Skp1ΔΔ

Figure S1

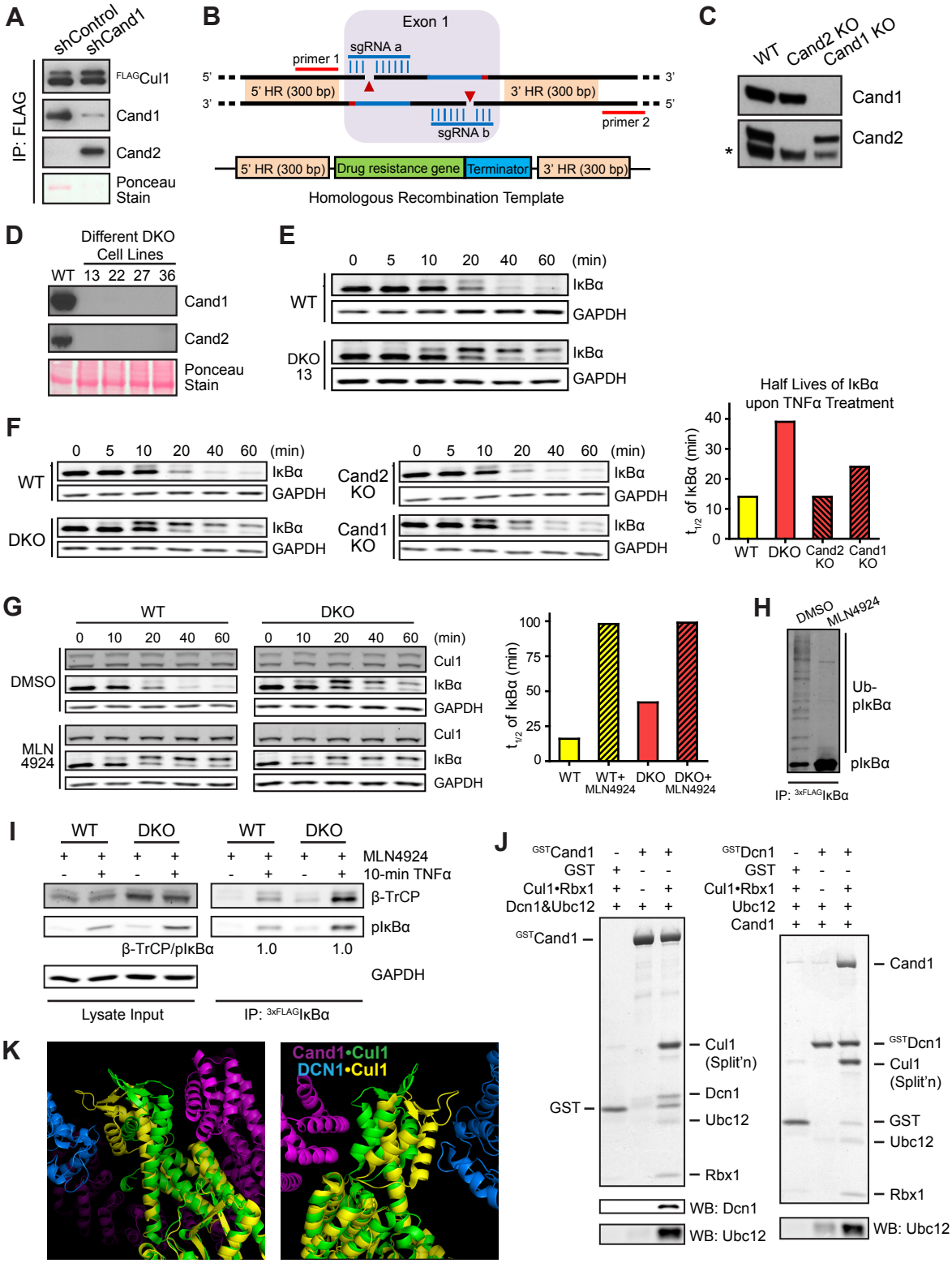
A
shControl
shCand1
IP: FLAG
FLAGCul1
Cand1
Cand2
Ponceau Stain
B
Exon 1
sgRNA a
primer 1
5'
3'
5' HR (300 bp)
3' HR (300 bp)
sgRNA b
primer 2
5' HR (300 bp)
Drug resistance gene
Terminator
3' HR (300 bp)
Homologous Recombination Template
C
WT
Cand2 KO
Cand1 KO
Cand1
Cand2
*
D
Different DKO Cell Lines
WT 13 22 27 36
Cand1
Cand2
Ponceau Stain
E
0 5 10 20 40 60 (min)
WT
DKO 13
IκBα
GAPDH
F
WT
DKO
Cand2 KO
Cand1 KO
IκBα
GAPDH
Half Lives of IκBα upon TNFα Treatment
t1/2 of IκBα (min)
WT DKO Cand2 KO Cand1 KO
G
WT
DKO
0 10 20 40 60 (min)
DMSO
MLN 4924
Cul1
IκBα
GAPDH
t1/2 of IκBα (min)
WT WT+ MLN4924 DKO DKO+ MLN4924
H
DMSO
MLN4924
Ub-pIκBα
pIκBα
IP: 3xFLAGIκBα
I
WT DKO WT DKO
MLN4924
10-min TNFα
β-TrCP
pIκBα
β-TrCP/pIκBα
1.0 1.0
GAPDH
Lysate Input
IP: 3xFLAGIκBα
J
GSTCand1
GST
Cul1•Rbx1
Dcn1&Ubc12
GSTDcn1
Ubc12
Cand1
Cand1
GSTDcn1
Cul1 (Split'n)
Dcn1
Ubc12
Rbx1
GST
WB: Dcn1
WB: Ubc12
K
Cand1•Cul1
DCN1•Cul1

Figure S2

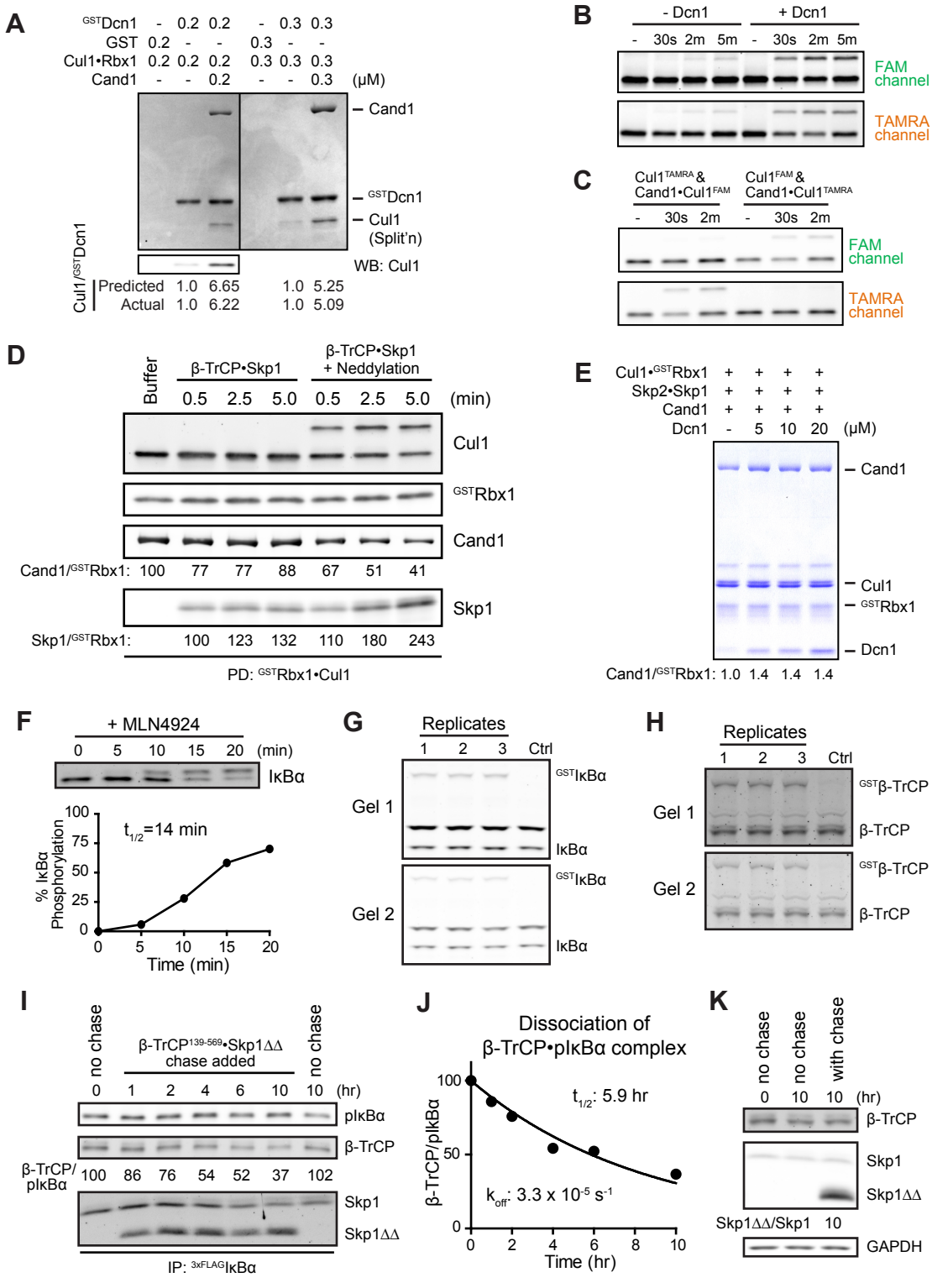
A
GSTDcn1 - 0.2 0.2 - 0.3 0.3
GST 0.2 - - 0.3 - -
Cul1•Rbx1 0.2 0.2 0.2 0.3 0.3 0.3
Cand1 - - 0.2 - - 0.3 (μM)
Cand1
GSTDcn1
Cul1 (Split'n)
WB: Cul1
Cul1/GSTDcn1
Predicted 1.0 6.65 1.0 5.25
Actual 1.0 6.22 1.0 5.09
B
- Dcn1
+ Dcn1
- 30s 2m 5m - 30s 2m 5m
FAM channel
TAMRA channel
C
Cul1TAMRA & Cand1•Cul1FAM
Cul1FAM & Cand1•Cul1TAMRA
- 30s 2m - 30s 2m
FAM channel
TAMRA channel
D
Buffer
β-TrCP•Skp1
β-TrCP•Skp1 + Neddylation
0.5 2.5 5.0 0.5 2.5 5.0 (min)
Cul1
GSTRbx1
Cand1
Cand1/GSTRbx1: 100 77 77 88 67 51 41
Skp1
Skp1/GSTRbx1: 100 123 132 110 180 243
PD: GSTRbx1•Cul1
E
Cul1•GSTRbx1 + + + +
Skp2•Skp1 + + + +
Cand1 + + + +
Dcn1 - 5 10 20 (μM)
Cand1
Cul1
GSTRbx1
Dcn1
Cand1/GSTRbx1: 1.0 1.4 1.4 1.4
F
+ MLN4924
0 5 10 15 20 (min)
IκBα
% IκBα Phosphorylation
t1/2=14 min
Time (min)
G
Replicates
1 2 3 Ctrl
Gel 1
Gel 2
GSTIκBα
IκBα
H
Replicates
1 2 3 Ctrl
Gel 1
Gel 2
GSTβ-TrCP
β-TrCP
I
no chase
β-TrCP139-569•Skp1ΔΔ chase added
no chase
0 1 2 4 6 10 10 (hr)
pIκBα
β-TrCP
β-TrCP/pIκBα 100 86 76 54 52 37 102
Skp1
Skp1ΔΔ
IP: 3xFLAGIκBα
J
Dissociation of β-TrCP•pIκBα complex
t1/2: 5.9 hr
koff: 3.3 x 10-5 s-1
β-TrCP/pIκBα
Time (hr)
K
no chase
no chase
with chase
0 10 10 (hr)
β-TrCP
Skp1
Skp1ΔΔ
Skp1ΔΔ/Skp1 10
GAPDH

Figure S3

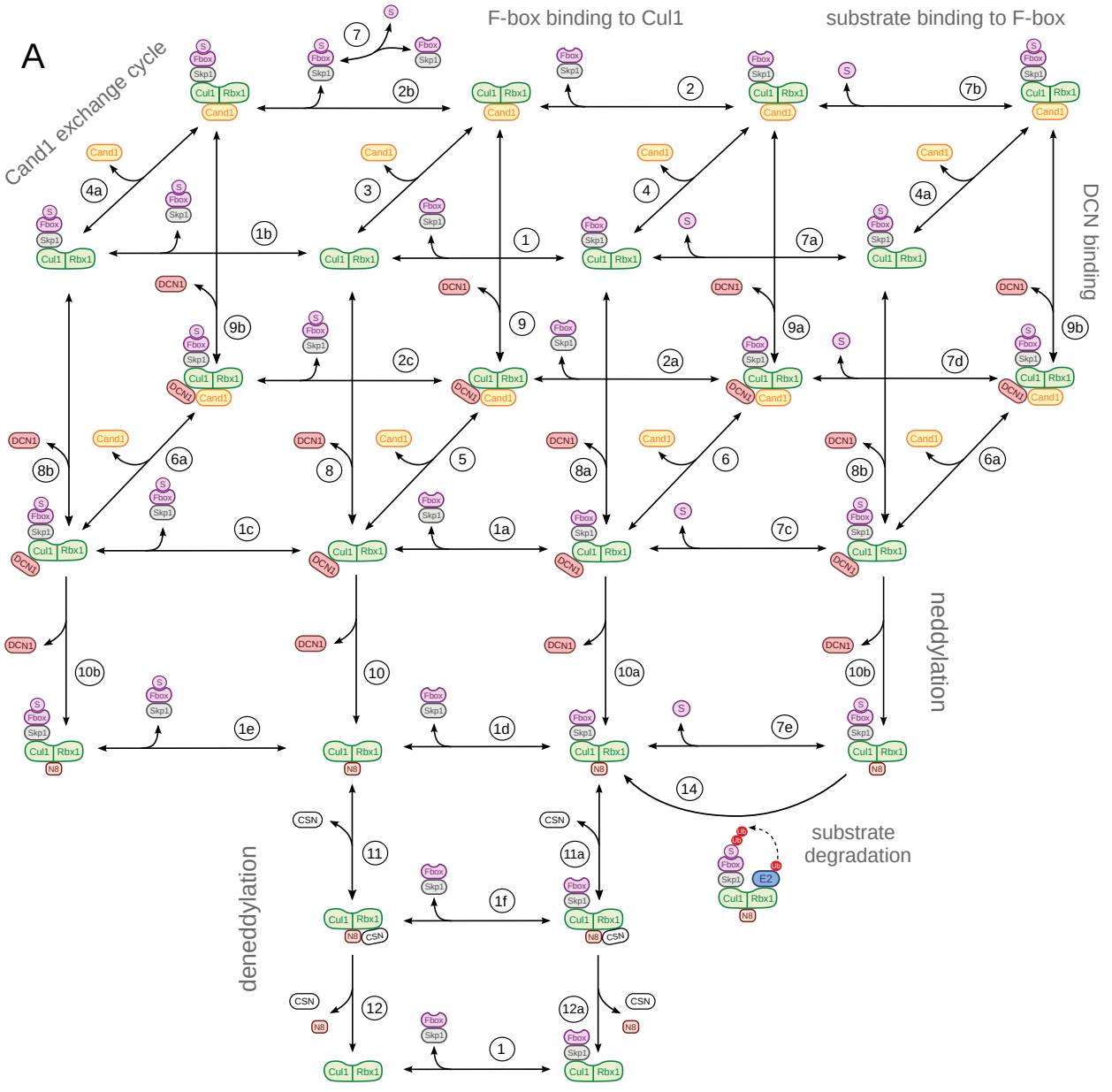
A
Cand1 exchange cycle
F-box binding to Cul1
substrate binding to F-box
DCN binding
neddylation
deneddylation
substrate degradation
B
product inhibition by CSN
C
detailed balance relations
$K_5 = \alpha K_3$
$K_9 = \alpha K_8$
K_8
K_3
K_1
$K_2 = \tau K_1$
$K_4 = \tau K_3$

Figure S4

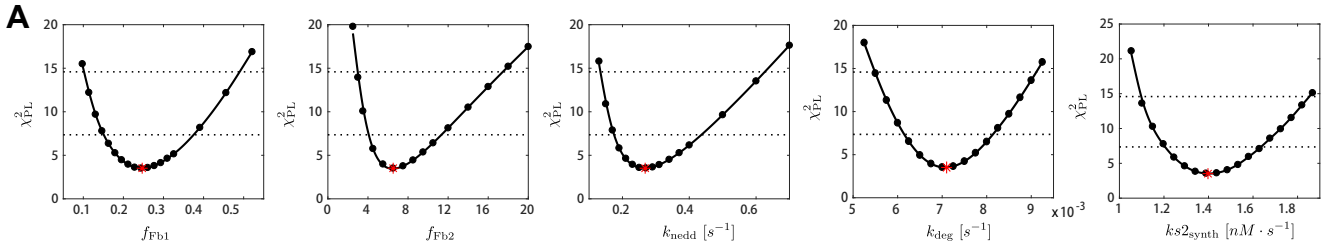

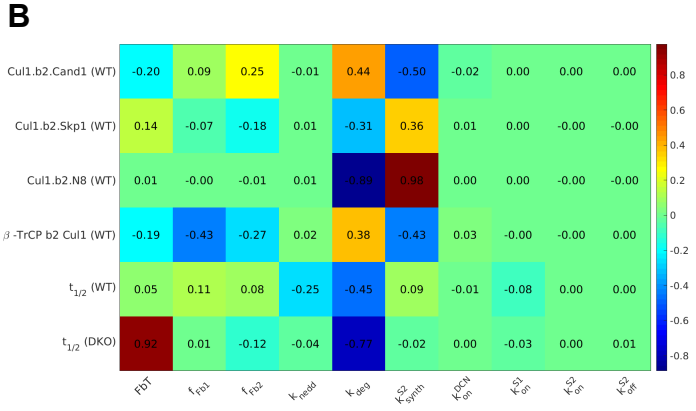

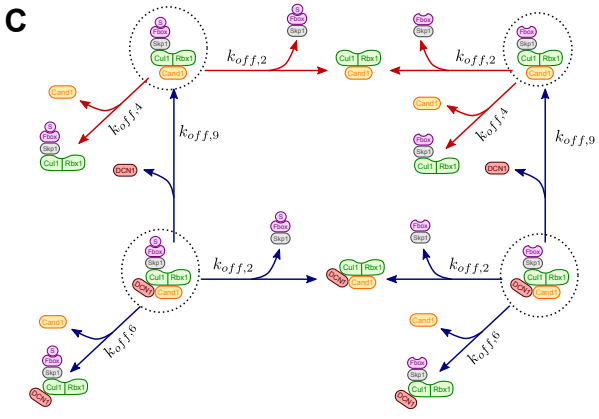

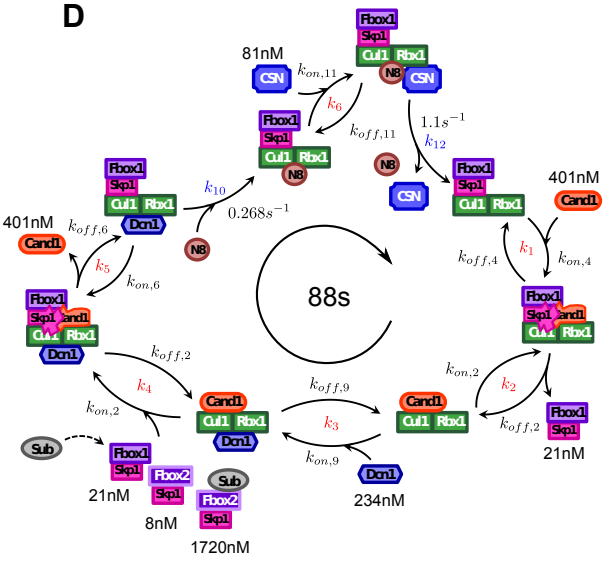

$(nM \cdot s)^{-1}$		s^{-1}		s^{-1}	
$k_{on,2}$	0.002	$k_{off,2}$	1.3	k_1	0.2
$k_{on,4}$	0.002	$k_{off,4}$	2.9	k_2	0.96
$k_{on,6}$	0.002	$k_{off,6}$	0.08	k_3	0.12
$k_{on,9}$	0.001	$k_{off,9}$	0.05	k_4	0.05
$k_{on,11}$	0.02	$k_{off,11}$	0.032	k_5	0.02
				k_6	1.57

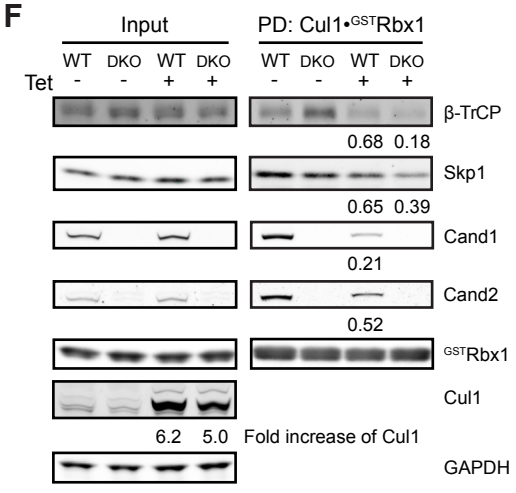

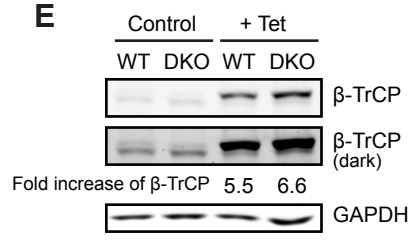

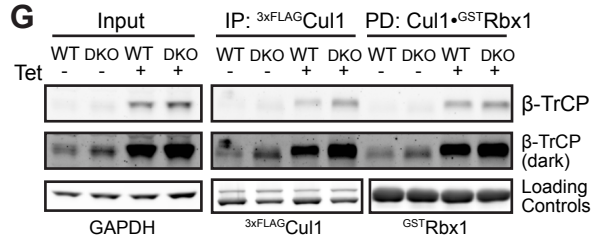

Figure S5

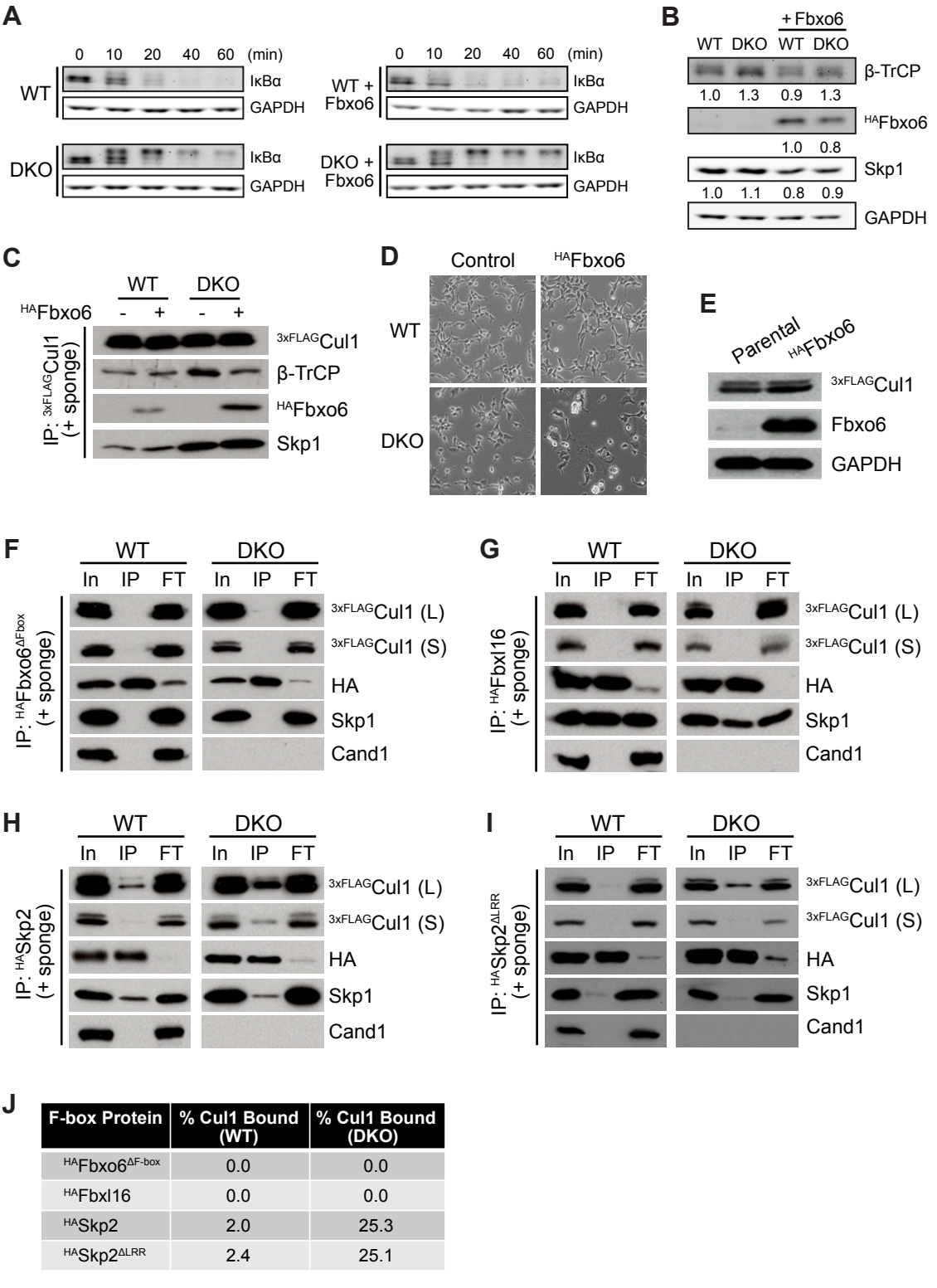

J

F-box Protein	% Cul1 Bound (WT)	% Cul1 Bound (DKO)
^{HA}Fbxo6$^{\Delta F\text{-box}}$	0.0	0.0
^{HA}Fbxl16	0.0	0.0
^{HA}Skp2	2.0	25.3
^{HA}Skp2$^{\Delta LRR}$	2.4	25.1

Figure S6

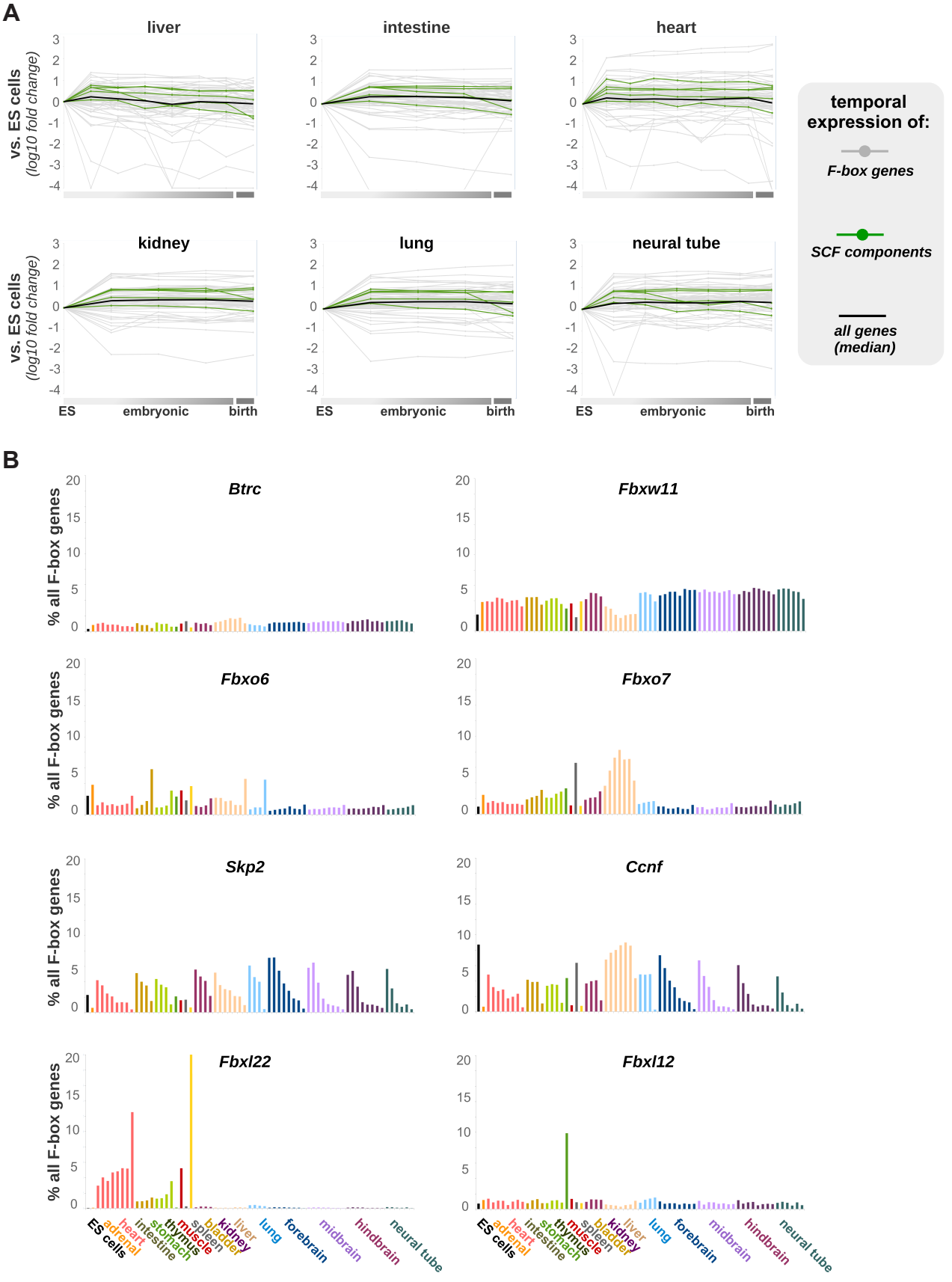
A
liver
intestine
heart
kidney
lung
neural tube
vs. ES cells
(log10 fold change)
ES
embryonic
birth
temporal expression of:
F-box genes
SCF components
all genes (median)
B
Btrc
Fbxw11
Fbxo6
Fbxo7
Skp2
Ccnf
Fbxl22
Fbxl12
% all F-box genes
ES cells
adrenal
heart
intestine
stomach
thymus
muscle
spleen
bladder
kidney
liver
lung
forebrain
midbrain
hindbrain
neural tube

Figure S7

SUPPLEMENTAL FIGURE LEGENDS

Figure S1. Properties of Cul1•Cand1 complex assembly and disassembly (related to Figure 1).

(A) k_{obs} for Cand1 binding to Cul1. The change in donor fluorescence versus time was measured in a stopped-flow fluorimeter upon addition of varying concentrations of $^{FlAsH\Delta H1}$Cand1 to 50 nM Cul1^{AMC}•Rbx1. Indicated concentrations are after 1:1 (v:v) mixing of the two solutions in the stopped-flow fluorimeter. Signal changes were fit to two phase exponential curves, and the fast-phase rates were used as k_{obs}. These values are plotted against [Cand1] in Fig 1B.

(B) k_{obs} for Cand1 binding to Cul1 preassembled with Skp1•Skp2. Similar to Fig S1A, except 100 nM Skp1•Skp2 was preincubated with 50 nM Cul1^{AMC}. Signal changes were fit to two phase exponential curves, and the fast-phase rates were used as k_{obs}. These values are plotted against [Cand1] in Fig 1C.

(C) k_{obs} for Cand1•Cul1 dissociation by Skp1•Skp2. The change in donor fluorescence versus time was measured in a stopped-flow fluorimeter upon addition of varying concentrations of Skp1•Skp2 to 10 nM $^{FlAsH\Delta H1}$Cand1•Cul1^{AMC}•Rbx1. Indicated concentrations are after 1:1 (v:v) mixing of the two solutions in the stopped-flow fluorimeter. Signal changes were fit to single exponential curves. These values are plotted against [Skp1•Skp2] in Fig 1E.

(D) Replacing the first helix of Cand1 with the tetracysteine tag increased the k_{off} of Cand1 from Cul1•Rbx1. Fluorescence emission at 445 nm (donor emission) was detected every 2 seconds after the addition of 10 x excess $^{FlAsH\Delta H1}$Cand1 (acceptor protein) to Cul1^{AMC}•Rbx1 pre-incubated with unlabeled Cand1 or $^{\Delta H1}$Cand1. FRET was observed following spontaneous dissociation of non-fluorescent Cand1 from Cul1^{AMC}•Rbx1. Signal changes were fit to exponential curves with a fixed end point of 70% initial donor fluorescence. Cand1•Cul1^{AMC}•Rbx1 was fit to a one phase curve. $^{\Delta H1}$Cand1•Cul1^{AMC}•Rbx1 was fit to a two phase curve, with $k_{off,\ slow}$ similar to the k_{off} of Cand1•Cul1^{AMC}•Rbx1 and $k_{off,\ fast}$ about 20 times faster.

(E) $^{\Delta H1}$Cand1•Cul1•Rbx1 is less stable than Cand1•Cul1•Rbx1. Skp1•Skp2, Cul1•^{GST}Rbx1, Cand1 or $^{\Delta H1}$Cand1 at indicated concentrations were used in the GST pulldown (PD) assay. Relative level of recovered Cand1 is shown as Cand1:^{GST}Rbx1 ratio. Based on this result and the known K_D of Cul1•Skp1•Fbxw7, the K_D of $^{\Delta H1}$Cand1•Cul1 is simulated to be ~4.5 times higher than the K_D of Cand1•Cul1. In this and other experiments employing recombinant Cul1, it migrates faster than expected because it is expressed by the 'split-n-coexpress' (split'n) method of Li et al (2005).

(F) β-TrCP removes Cand1 from Cul1 when it is in complex with full length Skp1 but not Skp1 with loop regions deleted. The change in donor fluorescence versus time was measured in a

stopped-flow apparatus upon addition of 75 nM Skp1•β-TrCP or Skp1ΔΔ•β-TrCP to 25 nM $^{FlAsH\Delta H1}$Cand1•Cul1^{AMC}•Rbx1.

(G) Deletion of β-hairpin in Cand1 or loop regions in Skp1 enables formation of a stable complex comprising Cul1, Skp1, and Cand1. *In vitro* pull-down assays containing the indicated proteins were performed to demonstrate the formation of stable complexes consisting of Cul1•Rbx1, Skp1 and ^{GST}Cand1 when Cand1 and/or Skp1 was mutated to delete structural elements that are predicted to clash in the Cand1•Cul1•Rbx1•Skp1 complex. The indicated proteins were mixed in equimolar amounts and bound to glutathione-4B resin. Proteins associated with the resin were fractionated by SDS-PAGE and detected by silver stain.

Figure S2. Degradation defects in Cand1Δ, Cand2Δ, and Cand1/2 double knockout cells (related to Figure 2). Complex of Cand1•Cul1•Dcn1 (related to Figure 3).

(A) Cand2•Cul1 complex was detected only when Cand1 was depleted. IP-WB analysis of Cand1•Cul1 and Cand2•Cul1 complexes in control (shControl) and Cand1 knock-down (shCand1) cells that are stably expressing the shRNA (Pierce et. al., 2013). Cells were treated with 1 μg/ml tetracycline for 1 hour 24 hours before collection to induce expression of ^{FLAG}Cul1 integrated at the FRT site (Flp-In system).

(B) Strategy for construction of Cand1/2 knockout cell lines. A pair of chimeric single-guide RNAs (sgRNA) guiding CRISPR Cas9 (D10A) nickases were designed to target the first exon of the Cand1 or Cand2 gene for mutagenesis. A homologous recombination (HR) template containing a drug resistance gene plus a translational terminator and two 300-bp homology arms that were identical to the genomic sequences flanking the first exon is depicted. Primer 1 and primer 2 were used to generate PCR products of the mutated genomic region for sequencing and confirming the complete inactivation of Cand1 and Cand2 genes. Note that primer 2 probed the region outside of the 300-bp HR region on the genomic DNA.

(C) Confirmation of Cand1 and Cand2 single KO cell lines. WB analysis showing the loss of Cand1 or Cand2 proteins in the corresponding KO cell lines. * marks a non-specific band, which serves as a loading control.

(D) Confirmation of Cand1/2 DKO cell lines. WB analysis showing the loss of Cand1 and Cand2 proteins in four DKO cell lines. DKO13, 22, 36 are independent cell lines confirmed by sequencing results. The filter stained with Ponceau S prior to probing is shown as a loading control. These lines initially displayed slower growth than the wild type (WT) cells, but the growth rate gradually increased after a few passages and became similar to the WT cells by the time their genotypes were confirmed.

(E) IκBα degradation is defective in DKO13 cells. WB analysis of IκBα levels in WT and DKO13 cells at indicated time points after TNFα treatment. DKO13 shows an IκBα degradation defect similar to the DKO22 and DKO36 lines shown in Fig 2A.
(F) Cand1 but not Cand2 is required for proper degradation of IκBα. WB analysis of IκBα degradation in response to TNFα treatment in WT, Cand1/2 DKO, Cand2 single knockout (Cand2 KO) and Cand1 KO cells. Half-lives of IκBα in this analysis are shown in the graph.
(G) Inhibiting neddylation stabilizes IκBα in both WT and DKO cells and enables quantification of the rate of IκBα phosphorylation. WB analysis of IκBα degradation in response to TNFα treatment in WT and DKO cells pretreated with either 0.1% DMSO or 1 μM MLN4924 for 1 hr. Half-lives of IκBα in this analysis are shown in the graph.
(H) Inhibiting neddylation strongly inhibits IκBα ubiquitination. Expression of ^{3xFLAG}IκBα cDNA integrated at the FRT site was induced with tetracycline for 24 hours and then ^{3xFLAG}IκBα was immunopreciptiated from cell lysate with anti-FLAG following pre-treatment of the cells with either 0.1% DMSO or 1 μM MLN4924 for 1 hr before 10-min TNFα treatment. IPs were evaluated by WB analysis with antibodies against pIκBα.
(I) pIκBα binds β-TrCP with equal efficiency in WT and DKO cells. WT and DKO cells expressing tetracycline-induced ^{3xFLAG}IκBα and treated with 1 μM MLN4924 for 1 hr to block pIκBα ubiquitination were lysed and subjected to IP with anti-FLAG followed by WB analysis with the indicated antibodies to evaluate interaction between pIκBα and β-TrCP. This is essentially the same as the experiment in Fig 2G, except that ubiquitination of pIκBα was suppressed by MLN4924, instead of by treating the IPs with deububiquitinating enzyme Usp2. MLN4924 or Usp2 were used to collapse all pIκBα species into a single band to facilitate quantification.
(J) Cand1 forms a complex with Dcn1 and Ubc12 only in the presence of Cul1. Reciprocal pull-down assays were set up as indicated. Each protein was included at 1 μM. Proteins adsorbed to the glutathione beads were fractionated by SDS-PAGE and stained by Coomassie blue or subjected to WB with the indicated antibodies.
(K) Binding of Cand1 alters the conformation of the Dcn1 binding site on Cul1. The C-terminal domains of Cul1 from PDB files of “4P5O” and “1U6G” were aligned in PyMOL, and the front and back views of the aligned Cand1•Cul1•Dcn1 are shown. Cand1 is in magenta and Dcn1 is in blue; Cul1 in complex with Cand1 is in green, and Cul1 in complex with Dcn1 is in yellow.

Figure S3. Cand1 and neddylation (related to Figure 3). Development of the computational model (related to Figure 4 and Method S1).

(A) Confirmation of the estimated K_D of 5 x 10^{-8} M for Dcn1 binding to Cand1•Cul1•Rbx1. Assays were similar to Fig 3C but lower concentrations of Cul1, Cand1 and ^{GST}Dcn1 were used. Proteins adsorbed to the glutathione beads were fractionated by SDS-PAGE and stained by Coomassie blue or subjected to WB with the Cul1 antibody. Fold increase of Cul1 recovered from the pulldown assay calculated by the K_D values (Predicted) and measured from the experiments (Actual) are shown.

(B-C) Negative controls for Fig 3F. (B) A mixture of 0.2 μM Cul1^{FAM} and 0.2 μM Cul1^{TAMRA} with or without 0.2 μM Dcn1 was incubated with 0.1 μM each of Nedd8, Ubc12, and NAE for indicated time period. FAM and TAMRA signals were detected by a Typhoon scanner.

(C) 5x Skp1•Skp2 and DKO lysate indicated in Fig 3E was replaced with 0.1 μM each of Nedd8, Ubc12, and NAE, and no FBP was added.

(D) Neddylation promotes the formation of SCF during the exchange process. Cand1, Dcn1 and Cul1•^{GST}Rbx1 were pre-incubated with glutathione beads and then mixed 1:1 (v:v) with protein solution containing Skp1•β-TrCP and Ubc12 or Ubc12~Nedd8. At indicated time points after mixing, beads were washed and eluted, and immobilized proteins were fractionated by SDS-PAGE and detected by WB. Final concentrations of the protein components were the same as in Fig 3G.

(E) Dcn1 stabilizes the Cand1•Cul1•Rbx1 complex in the presence of FBP. Pulldown analysis of recombinant Cand1 (1 μM) bound to recombinant Cul1•^{GST}Rbx1 (0.5 μM) in the presence of Skp1•Skp2 (2 μM) and increasing concentrations of Dcn1 (0-20 μM). Protein samples were fractionated by SDS-PAGE and stained with Coomassie Blue. Normalized levels of Cand1 recovered were calculated as the ratio of Cand1 to ^{GST}Rbx1.

(F) WB estimation of IκBα phosphorylation rate. WT cells were treated with 1 μM MLN4924 for 1 hr to inhibit the ubiquitination and degradation of pIκBα, and then sampled at indicated time points after TNFα treatment. The $t_{1/2}$ of IκBα phosphorylation is estimated to be 14 min.

(G-H) Concentration of endogenous IκBα is 10 times higher than endogenous β-TrCP. WB quantification of the endogenous IκBα (G) and β-TrCP (H) concentrations in WT cells, with recombinant ^{GST}IκBα (G) and ^{GST}β-TrCP (H) spiked into cell lysate as the internal standards. Three biological replicates were analyzed on two individual gels as technical replicates. The concentration of IκBα was estimated to be 650 ± 66 nM (SD, n=6). The concentration of β-TrCP was estimated to be 64 ± 6 nM (SD, n=6). In other experiments, sample titration was performed to confirm that the band intensities measured here were within the linear range of the instrument.

(I-K) pIκBα and β-TrCP form a very stable complex in cells. IP-WB analysis of the dissociation rate of the pIκBα•β-TrCP complex in cell lysate is shown in (I). DKO cell lysate containing 3xFLAG tagged pIκBα with or without added recombinant Skp1ΔΔ•β-TrCP$^{139-569}$ chase protein (~100x of endogenous β-TrCP level) was incubated at room temperature for indicated times. Dissociation of β-TrCP from pIκBα was calculated as ratios of β-TrCP to pIκBα signals in anti-FLAG IPs, and these ratios were used to estimate k_{off} (J) based on a fit to a single exponential. Lysate input for (I) is shown in (K). The amount of recombinant Skp1ΔΔ•β-TrCP$^{139-569}$ chase protein added was in large excess of total endogenous Skp1•FBP complexes as judged by relative signals for Skp1 and Skp1ΔΔ. In addition, the level of endogenous β-TrCP in the lysate remained constant throughout a10-hr incubation at room temperature with or without added chase protein.

Figure S4. Detailed reaction scheme of the SCF cycle model (related to Figure 4 and Method S1).

(A) The scheme depicts the state variables and the reactions in the network as listed in Method S1 (Tables T2-T13). Fbox and S denote either Fb1 and S1 (relating to β-TrCP and pIκBα) or Fb2 and S2 (relating to auxiliary substrate receptors and their substrates). Lines with unidirectional arrows represent irreversible reactions. Reactions labeled by the same number (but different lower case letters) have the same kinetic parameters (Tables T3-T13 of Method S1). Note that for better visibility some states are drawn twice in the network.

(B) Reactions describing product inhibition of CSN by unneddylated Cul1 species. We assume that states in which Cul1 is not neddylated and its associated FBP is not bound to substrate, can bind CSN leading to the formation of complexes which are devoid of SCF ligase activity.

(C) Illustration of the detailed balance relations for the thermodynamic cycles involving Cand1 and FBP (lower cycle, $K_1K_4 = K_2K_3$), and Cand1 and Dcn1 (upper cycle , $K_8K_5 = K_3K_9$) (see Method S1 for details).

Figure S5. Parameter identifiability analysis, response matrix, computation of protein fractions and cycle time (related to Figure 4, Figure 7 and Method S1). Experimental tests of the mathematical model predictions (related to Figure 5).

(A) Profile likelihood as a function of estimated parameters (Table T15 of Method S1). Circles were determined by numerically computing the profile likelihood according to Eq. (S10). Red circles represent the optimal parameter values that minimize χ^2 as defined in Eq. (S9). Solid lines are smooth interpolations of the data points. Horizontal dotted lines represent thresholds

as defined in Eq. (S11) that were used to derive 95% confidence intervals, either pointwise (lower line) or simultaneous (upper line).

(B) Matrix of response coefficients as defined by Eq. (S12) (see Method S1). Parameters on the horizontal axis were increased by 10% and the relative change of different observable quantities (vertical axis) was computed. Positive / negative response coefficients indicate a positive / negative correlation between parameter and observable quantity. Absolute values larger (smaller) than 1 indicate a high (low) sensitivity with respect to the corresponding parameter. The greater the absolute value of a response coefficient, the more sensitive the respective quantity is to changes in the corresponding parameter. Parameters are defined in Table T15 of Method S1. The abbreviation “b2“ means “bound to“.

(C) The scheme illustrates the computation of the coefficients defined in Eqs. (S13) and (S14) which determine the contribution of the encircled protein complexes to the protein fractions Cand1.b2.Cul1 and Skp1.b2.Cul1 as defined in Table T14 of Method S1. Note that these complexes are unstable (since they contain both Cand1 and FBP), and thus cannot be detected in our pull-down assays. Fb and S may denote Fb1 (β-TrCP) and S1 or Fb2 (auxiliary SRs) and S2.

(D) Illustration of the computation of the cycle time according to Eq. (S21). Concentrations represent steady state concentrations of free (unbound) proteins obtained from simulations using parameters for WT cells (Table T2-T13, T15 of Method S1). Numbers in the table summarize the values of the on and off rate constants as well as the corresponding net rate constants (red color) computed from Eqs. (S15) - (S20).

(E) Confirmation of β-TrCP overproduction in Fig 5C by WB analysis. Fold increase in total β-TrCP levels are indicated. (dark): more intense exposure of β-TrCP blot. A 9-fold increase in total β-TrCP level in both WT and DKO cells was observed in a replicate experiment.

(F) Overexpression of ^{3xFLAG}Cul1 reduces levels of unassembled cellular β-TrCP, Cand1 and Cand2. As depicted in Fig 5D, WT and DKO cells were treated with or without tetracycline to induce expression of a stably integrated ^{3xFLAG}Cul1 transgene, and then lysed in the presence of excess Cul1•^{GST}Rbx1 to capture unassembled β-TrCP, Skp1, Cand1, and Cand2. Lysates were subjected to pulldown with glutathione beads, and bound fractions were subjected to WB with the indicated antibodies. One set of representative results from two replicate experiments are shown. These are the underlying data for the graph in Fig 5E.

(G) Overproduction of β-TrCP modestly reduces the efficiency of its assembly with Cul1. As depicted in Fig 5F, WT and DKO cells with 3xFLAG-tagged endogenous Cul1 were treated with or without tetracycline to induce expression of a stably integrated β-TrCP transgene, and then

lysed in the presence of excess Cul1•^{GST}Rbx1 to suppress Cand1-mediated exchange and capture unassembled Skp1•β-TrCP complexes. Lysates were subjected to IP with anti-FLAG followed by pull-down with glutathione beads. Bound fractions were subjected to WB with the indicated antibodies. One set of representative results from two replicate experiments are shown. These are the underlying data for the graph in Fig 5G.

Figure S6. FBP-dependent sequestration of Cul1 inhibits proliferation of DKO cells (related to Figure 6).

(A-B) Fbxo6 overexpression further slows IκBα degradation rate in the DKO cells. These are the underlying data for the graph in Fig 6A. Cells were infected with lentiviruses to overproduce Fbxo6 and were subjected to TNFα treatment three days after the viral infection.

(B) WB analysis of β-TrCP, ^{HA}Fbxo6, and Skp1 in the cell lysates from panel (A). Relative protein levels are indicated below each blot.

(C) Overproduction of ^{HA}Fbxo6 decreases the endogenous SCF$^{β\text{-}TrCP}$. ^{3xFLAG}Cul1 was immunoprecipitated from WT and DKO cells overexpressing ^{HA}Fbxo6 in the presence of recombinant Cul1•^{GST}Rbx1 (+ sponge). Co-immunoprecipitated β-TrCP and ^{HA}Fbxo6 were analyzed by WB.

(D) Overexpression of Fbxo6 alters the morphology of DKO cells. Live cell images were acquired at 20x magnification seven days after viral infection.

(E) WB with anti-Fbxo6 antibody showing ^{HA}Fbxo6 overproduction five days after infection with recombinant lentivirus. The overproduction is estimated to be 45 times of the endogenous level.

(F-I) Co-IP of ^{3xFLAG}Cul1 with overexpressed ^{HA}Fbxo6^{ΔFbox} (F), ^{HA}Fbxl16 (G), ^{HA}Skp2 (H), and ^{HA}Skp2^{ΔLRR} (I) in the presence of recombinant Cul1•^{GST}Rbx1 (+ sponge). Cells were infected by lentiviruses to overexpress different FBPs, and the experimental procedures were similar to Fig 6D. Long (L) and short (S) exposures of endogenous ^{3xFLAG}Cul1 are shown.

(J) Quantification of the relative percent of Cul1 co-immunoprecipitated with overexpressed FBPs in (F-I), n = 2.

Figure S7. FBP expression is dynamic during mouse development (related to Figure 6 and Discussion).

(A) Expression of FBP genes is highly variable during development of multiple tissues, despite stable expression of core SCF components. RNA-seq data from ENCODE for the indicated tissues during mouse development were normalized to ES cell expression levels. Fold change for each embryonic and birth timepoint relative to ES cells is presented in log10 scale. Each

datapoint is derived from FPKM RNA-seq values and is the average of two replicates. Grey datapoints and lines represent expression of 73 FBPs, green represents SCF complex components (Cul1, Rbx1, Skp1, Cand1, and Cand2), and black represents the median fold change for all transcripts expressed in ES cells (25130 transcripts).
(B) Expression of many FBPs is highly dynamic during development. RNA-seq data from ENCODE for mouse development was obtained as FPKM values, and averaged for two replicates. For selected FBPs, expression levels relative to total expression of 73 FBPs was calculated for each tissue and timepoint. Distinct colors represent different tissues as listed on the bottom, and bars in the same color represent different embryonic developmental timepoints from early organogenesis (leftmost; timepoint varies by tissue) to birth (rightmost). Tissues with only one timepoint represent gene expression at birth.